Article

Kinetic Roughening of Glucose Isomerase Crystals

Mike Sleutel, Dominique Maes, Lode Wyns, and Ronnie Willaert

Cryst. Growth Des., **2008**, 8 (12), 4409-4414 • Publication Date (Web): 08 November 2008

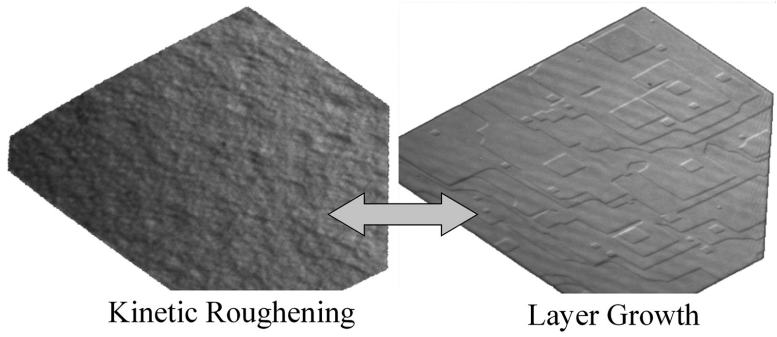

More About This Article

Additional resources and features associated with this article are available within the HTML version:

- Supporting Information
- Access to high resolution figures
- Links to articles and content related to this article
- Copyright permission to reproduce figures and/or text from this article

View the Full Text HTML

CRYSTAL GROWTH & DESIGN
2008
VOL. 8, NO. 12
4409–4414

Kinetic Roughening of Glucose Isomerase Crystals

Mike Sleutel,* Dominique Maes, Lode Wyns, and Ronnie Willaert

Ultrastructure, Flanders Interuniversity Institute for Biotechnology (VIB), Vrije Universiteit Brussel, Belgium

Received December 12, 2007; Revised Manuscript Received April 1, 2008

Ⓦ **This paper contains enhanced objects available on the Internet at http://pubs.acs.org/crystal.**

ABSTRACT: Protein crystals grow by the incorporation of growth units from solution into the crystal bulk. At low supersaturation, growth sites are kinks at step edges that are generated through the formation of spiral dislocations and/or two-dimensional (2D) nucleation. At conditions farther away from equilibrium, a critical supersaturation σ_R can be reached where the critical 2D nucleus equals a single growth unit. As a result, each surface site becomes a potential growth site, making growth fast and the surface rough. This transition from layer-by-layer growth to a faster random addition of solute molecules to the surface, that is, kinetic roughening, was visualized using laser confocal microscopy combined with differential interference contrast microscopy for the case of glucose isomerase. Evidence for continuous growth is presented at σ_R: the critical nucleus is predicted to be the size of 2 glucose isomerase tetramers and normal face growth velocities switch from a nonlinear to a linear relationship with the supersaturation. Moreover, at supersaturation higher than σ_R, rounding of crystal facets occurs. From this we conclude that glucose isomerase transitions at $\sigma_R = 5.0 \pm 0.1$ to a continuous growth mechanism characterized by an energy barrier of $3.74 \pm 0.01 \times 10^{-13}$ erg/molecule at 20 °C.

Introduction

For the case of macromolecular crystallization, crystal growth takes place at the crystal−solution interface. The mechanism of crystal growth is unambiguously determined by the structure of the crystal surfaces. Relatively rough surfaces, such as S (stepped) and K (kinked) faces,[1,2] offer enough kink sites to ensure their growth and hence grow fast. The structure of F (flat) faces[2] of perfect crystals, however, offers no kink sites and rely on kink generating mechanisms to procure their growth. Owing to the substantial kink density in K faces and to a lesser extent in S faces, it follows that during growth these two types of faces disappear first, giving rise to a crystal fully enclosed by low index F faces.[3] Below the roughening temperature T_R, the overall crystallographic orientations of these F-faces are generally maintained. Faceted interfaces are smooth on a molecular scale and growth proceeds by the attachment of new growth units into kink sites along step edges. New step edges are created by screw dislocations intersecting the interface, through the formation of two-dimensional (2D) nuclei and the incorporation of microcrystals.[4−9] If the temperature is equal to or above T_R, the step edge free energy vanishes and the crystal surface becomes rough at a molecular scale and undergoes a thermodynamic phase transition, called *thermal roughening*.[10−15]

At $T < T_R$, the step edge free energy is larger than zero. Consequently, according to the classical nucleation theory,[16] a nucleation barrier for the formation of the critical two-dimensional nucleus exists and with it a critical nucleus size larger than the crystal's individual building blocks. The size of this critical nucleus is inversely proportional to the temperature and the supersaturation. At a constant temperature, an increase in the supersaturation will translate into a decrease in critical nucleus size. As a consequence, in spite of the nonzero step edge free energy, a critical supersaturation σ_R will exist for which the barrier for 2D nucleation essentially vanishes and the size of the critical 2D nucleus is reduced to the order of one growth unit. Due to a large step density and a very small 2D critical nucleus at elevated supersaturations, the surface becomes rough and offers many favorable sites uniformly distributed across the surface. Consequently, arriving molecules can be incorporated quasi at any site. This transition from a slow, layer-by-layer growth regime to a fast continuous growth regime at high driving forces is called the *kinetic roughening* transition.[17−22] Kinetic roughening for the case of crystallization from solution has been observed for many small molecules, that is, SiO_2,[23] Al_2O_3,[24] ZnO, and ZnS,[25,26] n-paraffins[27,28] and many others. For the case of protein crystallization, continuous growth has only been observed for lysozyme[29−31] and apoferritin.[6]

In this paper we will discuss kinetic roughening for the case of the protein glucose isomerase. The first section deals with the difference in growth kinetics at low and high supersaturation levels (i); in what follows we present quantitative data for both the classical layer-by-layer growth mechanism at low supersaturation (ii) and the kinetic roughening regime at high supersaturation (iii).

Materials and Methods

A. Crystallization of Glucose Isomerase. Glucose isomerase from *Streptomyces rubiginosus* was purchased from Hampton Research (California, USA). The protein solution was dialyzed against 10 mM Hepes buffer pH 7.0 and 1 mM $MgCl_2$. Protein concentrations were determined by UV absorbance at 280 nm. For the interferometry experiments, protein crystals were grown in situ inside the Mach−Zehnder interferometer (MZI) in a Hellma fluorescence cuvette (Jena, Germany) kept at a constant 20 °C using the batch method. Mother liquor consisted of 40 mg/mL glucose isomerase, 100 mM Hepes pH 7.0, 200 mM $MgCl_2$, 5% PEG 1000 and 0.1% LM agarose (Hampton) to inhibit convective flows. For the atomic force microscopy (AFM) experiments, crystals were grown at 20 °C on nonsiliconized 10 mm diameter glass discs using the sitting drop vapor diffusion technique with the aid of microbridges (Hampton Research). The protein solution used in the crystallization set-ups contained 30 mg/mL protein in 100 mM Hepes pH 7.0 and 200 mM $MgCl_2$. Drops were prepared by mixing 2 μL of glucose isomerase solution with 2 μL reservoir solution of 100 mM Hepes pH 7.0, 200 mM $MgCl_2$ and 5% PEG 1000. For these conditions,

* To whom correspondence should be addressed. E-mail: mike.sleutel@vub.ac.be. Telephone: +32-2-6291923. Fax: +32-2-6291963.

10.1021/cg701220t CCC: $40.75
Published on Web 11/08/2008

the protein crystallizes in the orthorhombic form (*I*222, $a = 94.01$ Å, $b = 99.37$ Å, $c = 103.01$ Å).[32]

B. Protein Depletion Zone Characterization. Protein concentration gradients were measured using a computer controlled MZI-microscopy system (680 nm) using a quartz fluorescence cuvette as experimental cell with inner dimensions 10 mm × 4 mm × 45 mm (D × W × L). The experimental cell was placed in the interferometer in the object beam trajectory and kept at 20 ± 0.1 °C using Peltier elements in combination with coolant water flows at the sides of the experimental cell. Phases were obtained using the phase-shift method. Phase-shifts were induced by a piezo connected to the object beam mirror. Using the Hariharan algorithm[33] phase interferograms could be reconstructed. Real phase values were obtained by subtracting the reference phase field (taken at the start of the experiment) from each phase map. Phase difference maps were transformed into concentration difference maps by using refractive index versus concentration calibration curves determined using an Abbe Refractometer model 60/ED. Such a conversion from refractive indices to protein concentrations does however require that the phase difference between two successive interferograms is smaller than one corresponding wavelength. This was ensured by conducting the time-lapse imaging at a frame rate of 1 frame/15 min. The obtained raw data represents the integration of the protein concentration along the optical path, and as such are averaged values. Assuming a spherical depletion zone,[34] the error introduced through this integration can be estimated by using the correction proposed by Otalora et al.[35] For realistic values of the following parameters, face kinetic constant $\beta_{face} = 5 \times 10^{-5}$ cm/s, bulk diffusivity $D_{bulk} = 4 \times 10^{-7}$ cm^2/s, protein concentration $C_{bulk} = 40$ mg/mL, protein equilibrium concentration $C_{eq} = 0.22$ mg/mL, an optical path length of 2 mm and a varying crystal size from 10−1000 μm, Otalora's model predicts on average an error of 5% for the surface concentration. This error remains reasonable and the data derived from the MZI will be used without correction. For larger crystal sizes however, the error can be as large as 20%. Hence, data for crystal sizes larger than 1 mm were discarded.

C. Face Growth Velocity Measurements Using Mach−Zehnder Interferometry. Face growth velocities were extracted from the intensity data recorded with the MZI. From these interferometric images, we recorded observations of changes in linear dimensions of specific facets of crystals as a function of time. The slope of the observed linear dimension versus time determined the normal crystal growth velocity.

D. Step Growth Velocity Measurements Using Atomic Force Microscopy (AFM). AFM imaging of the crystallization processes was conducted in tapping mode using Nanoscope IIIa multimode AFM (Veeco, Santa Barabara, USA). Images were recorded in buffer solutions of identical composition to the mother liquor, but at varying protein concentrations (0.5−40 mg/mL). Because the equilibrium glucose isomerase concentration C_{eq} at 5% PEG 1000, obtained from the measured solubility curve is sensitive to temperature changes, the sample temperature was measured in situ while scanning the surface. Standard silicon nitride and oxide sharpened SPM tips (Veeco, Santa Barabara, USA) were used. Cantilevers with nominal force constants of 0.01 N/m were typically utilized. In order to minimize the force applied to the crystalline surface during scanning, the set point voltage was continually adjusted to the lowest level for which tip-crystal contact was maintained. Step growth velocities were determined by scanning perpendicular to the step and disabling the slow scan (vertical) axis. The slopes of the steps were taken as the tangential growth velocities.

E. Growth Mechanism Identification Using Laser Confocal Microscopy (LCM) Combined with Differential Interference Contrast Microscopy (DIM). Growing (011) faces of orthorhombic glucose isomerase crystals were observed in situ by LCM-DIM.[36] For this, a D-Eclipse C1 confocal system was attached to an inverted Eclipse TE-2000 U optical microscope (Nikon, Japan). An air objective lens PlanFluor 20× with a numerical aperture of 0.45 and a working distance of 7.6 mm was used (lateral resolution 660 nm). The diameter of the confocal aperture used for the observation was 103 μm. A Nomarski prism was inserted into the optical path to utilize differential interference contrast. The experimental cell was a 45 mm × 12.5 mm quartz cuvette with two detachable windows (Hellma, Müllheim, Germany). Crystals were illuminated with an argon-ion laser with a wavelength of 488 nm. Photomicrographs of 512 × 512 pixels were acquired over a 4 s scan time with a pixel-dwell of 11 μs and the images were recorded as fast as possible given the high growth velocities for elevated supersaturation levels. Crystals were grown in situ using the batch method at 30 mg/mL glucose isomerase, 100 mM Hepes pH 7.0, 200 mM $MgCl_2$ and 5% PEG1000. Protein crystals were obtained within minutes after sample preparation and LCM-DIM data collection started immediately. Next, one (011) face was observed using LCM-DIM for several days.

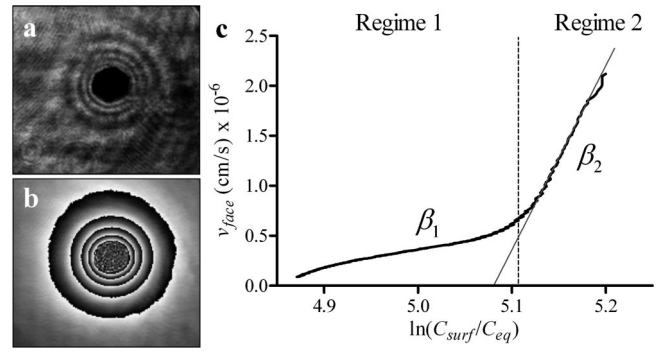

Figure 1. Recorded intensity (a) and phase shift interferograms (b) of the isotropic depletion zone encircling the glucose isomerase crystal; growth face velocities v_{face} of glucose isomerase at 100 mM Hepes pH 7.0, 200 mM $MgCl_2$, 5% PEG 1000, 0.1% agarose at 20 °C. A clear transition from *slow* (regime 1) to *fast* (regime 2) kinetics is observed for elevated supersaturation levels (c).

Results and Discussion

(i) Crystal Face Velocities Show an Acceleration in Kinetics at High Supersaturation Levels. Because of the presence of 0.1% agarose in the experimental MZI conditions, convective flows are effectively inhibited,[37,38] and a diffusive growth environment is installed. Under such diffusion driven mass transport conditions, the concentration gradient build-up adjacent to the crystal face is maintained and leads to the formation of an isotropic protein depletion zone (Figure 1a,b). This metastable halo encircling the crystal creates local solutal conditions that can differ greatly from the bulk supersaturation. As crystal growth proceeds, the crystal experiences a lower interfacial supersaturation and hence, a lower growth rate. Consequently, for the growth of a single crystal, a multitude of supersaturation levels and the accompanying face growth rates can be sampled.

Using MZI, we are able to determine the protein concentration at the surface during the crystal growth process. Using the obtained values for the measured surface protein concentration recorded over the course of the experiment, the supersaturation dependence of the crystal face velocity is obtained (Figure 1c). Figure 1c clearly shows two distinctly different growth regimes as a function of supersaturation, possibly emanating from two different growth mechanisms with varying rate constants as a function of supersaturation. This transition from *slow* to *fast* kinetics is observed for all the faces of the crystal presented in Figure 1a. However, the exact transition concentration and the corresponding slopes may vary. Repetitions of the experiment (9 crystals, 49 crystal faces) show that this transition is crystal size independent and occurs at a supersaturation $\sigma = \ln(C_{surf}/C_{eq}) = 5.0 \pm 0.1$ with C_{surf} the protein concentration and C_{eq} the equilibrium concentration.

In a first approach, the growth rate of the crystal faces was evaluated using the following basic model for crystal growth[39]

$$v_{face} = \Omega \beta_{face} (C_{surf} - C_{eq}) \quad (1)$$

with v_{face} the growth rate of the crystal face (cm/s), Ω the specific volume of a single glucose tetramer in the crystal lattice

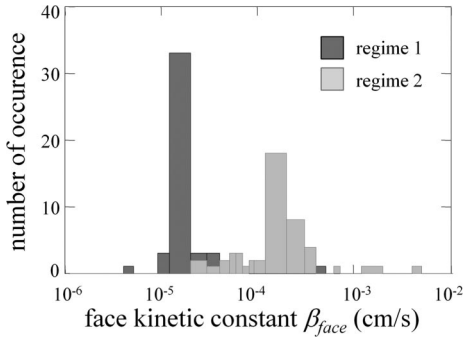

Figure 2. Histogram of the face kinetic constant β_{face} for glucose isomerase, with dark gray solid bars corresponding to regime 1 as shown in Figure 1c and light gray solid bars to regime 2.

(4.99×10^{-19} cm^3), and C_{surf} and $C_{eq} = 7.7 \times 10^{-14}$ cm^{-3} the protein surface and equilibrium concentration, respectively. The analysis of the MZI data using eq 1 yielded the histogram for β_{face} depicted in Figure 2a. As can clearly be seen, the slow and fast kinetic growth regimes translate into roughly 1 order of magnitude difference for the corresponding face kinetic constants β_{face}.

(ii) Growth Mechanism at Low Supersaturation. Layer-by-Layer Growth. The growth mechanism for the low supersaturation range from 0.8−3.5 was identified using AFM. At higher driving forces, heterogeneous nucleation takes place within the fluid cell and stable measuring conditions are lost. For the precipitant PEG 1000, the dominating layer generation mechanism at low supersaturation is 2D nucleation (Figure 3a). Although spiral dislocations have been reported for the growth of glucose isomerase crystals using the precipitants PEG 400,[40] no spiral dislocations were observed in this study. The presence of step bunching resulting in large macrosteps with highly varying local slopes was also recorded (Figure 3c). The lattice spacing between the 2D unit cells was determined with AFM to be $a \sim 10$ nm, $b \sim 9$ nm with a step height of 7 nm (Figure 3b). This corresponds relatively well with the values obtained from the X-ray structure[32] of the (011) face, $a_{cryst} = 100$ Å, $b_{cryst} = 93.80$ Å. The step velocities as a function of supersaturation were measured using AFM. Using these velocities, the step kinetic coefficient was estimated from the slope of the curve in Figure 4, giving for $\beta_{step} = 1.2 \times 10^{-3}$ cm/s.

In a narrow supersaturation range, the crystallization kinetics of regime 1 can be approximated as being linear. However, if we combine the MZI-obtained velocities for small supersaturations with the recorded AFM data, a nonlinear relationship of the growth face velocities with the supersaturation is found (Figure 5). In order to combine the MZI data with the AFM step velocities we need to multiply the step velocities with the crystal slope p to obtain the face growth velocities. For this, we use an experimentally determined (AFM) average value of the local crystal slope ($p = 0.005 \pm 0.004$). We can now evaluate these velocities with a more in-depth model, that is, the expression for face growth rates in case of two-dimensional nucleation[41] and estimate the effective energy barrier γ and the frequency A,

$$v_{face}(C,T) = AC_{eq}^{1/3} \exp\left(\frac{2}{3}\sigma\right)\sigma^{1/6}(\exp\sigma - 1)^{2/3} \times \exp\left(-\frac{\pi\gamma^2}{3\sigma(k_BT)^2}\right) \text{ and } \gamma = \kappa\Omega_{surf}^{1/2} \quad (2)$$

with A the frequency at which a macromolecule attempts to overcome a barrier (s^{-1}), γ the effective step free energy (erg/molecule), Ω_{surf} the attachment unit area at a lattice site (nm^2), and κ the step energy per unit length (erg/nm). In Figure 5 we have combined both the MZI face velocities and the AFM step velocities multiplied by the crystal slope p. From this kinetic data, we obtain the effective energy barrier $\gamma = 1.43 \pm 0.01 \times 10^{-13}$ erg/molecule and the frequency $A = 6.2 \pm 0.2 \times 10^{-14}$ s^{-1} (goodness of fit $R^2 = 0.9965$). Note the inability of eq 2 to predict face kinetics at high supersaturation levels. This suggests that 2D nucleation might not be the dominating layer generation mechanism at such driving forces in regime 2.

(iii) Kinetic Roughening Transition from 2D Nucleation to Continuous Growth. In the interferometry experiments a striking increase in kinetics is observed when reaching $\sigma_R = 5.0 \pm 0.1$. Such an acceleration might indicate that a new growth mechanism starts to dominate the previous ruling one. Using LCM-DIM, a direct visual identification of the growth mechanism at these high supersaturation levels is possible (Figure 6). A transition from layer-by-layer growth through 2D nucleation to a continuous growth mechanism can be seen in Figure 6f-a. This transition is characterized by a decrease in critical 2D nucleus size and an increase in 2D-nucleation rate resulting in a rough surface on which no steps can be discerned (for a time-lapse movie of this transition, see additional information).

Time-lapse imaging of Figure 6a,b (movie1.avi), time-lapse imaging of Figure 6c,d,f (movie2.avi), and time-lapse imaging showing a clear difference between kinetic roughening and 2D nucleation (movie3.avi) are available in the online version of this paper.

To our knowledge, there is only one theoretical model present in the literature that predicts crystal growth rates at elevated driving forces below the roughening temperature, and this is the model of kinetic roughening. Since kinetic roughening is not an actual phase transition, but rather a kinetic phenomenon, it lacks a precise definition.[42] Consensus does exist however on the criteria that may be employed to identify it:[42] (i) a critical supersaturation σ_R exists for which the barrier for 2D nucleation essentially vanishes and the theoretical critical radius becomes smaller than half a growth unit; (ii) above σ_R face kinetics are expected to follow a linear relationship with the supersaturation; (iii) kinetic roughening coincides with the observed transition from flat to rounded crystal facets. In the following paragraphs we shall address these 3 criteria for the crystallization of glucose isomerase.

Critical Radius of the Two-Dimensional Nucleus. Because of the very small nature of the critical 2D nucleus for the case of kinetic roughening, growth units can nucleate in kinks, on step edges, and terraces. Therefore, growth proceeds by the random addition of solute molecules to the crystal surface. Consequently, the notion of a *step* and a *terrace* is no longer applicable. The onset of this process occurs when the static mean excursion of an isolated step w is larger than the mean terrace width. To verify this assumption, we measured the average width w of isolated steps at equilibrium (5% PEG 1000, $C_{eq} \sim 1$ mg/mL) using AFM. The step width scales with the length of the observed step, so for a broad range of measured step lengths, a spread on w is expected. Nonetheless, we obtained $w = 40 \pm 8$ nm (95% confidence interval). Next, we determined the average terrace width as a function of supersaturation (Figure 7a). As can clearly be seen from Figure 7a, the interstep distance decreases steadily as a function of supersaturation. At $\sigma \sim 3.8$, the distance between the steps narrows down to the width of a single step. For more elevated supersaturation levels, this trend predicts an even greater decline in terrace width, hence corroborating the notion that steps will start to merge and

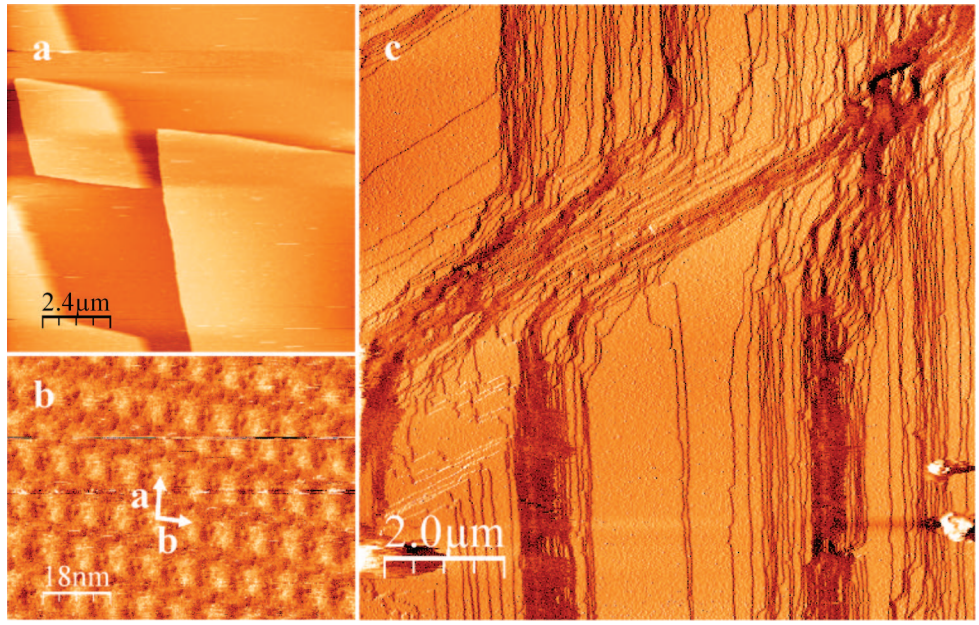

Figure 3. The growth mechanism for glucose isomerase at low to moderate supersaturation (regime 1 in Figure 1c) as imaged using AFM. (a) Two-dimensional nucleation on the (011) face (height image); (b) molecular resolution image showing intermolecular vectors *a* (9 nm) and *b* (10 nm) (height image); (c) step bunching resulting in the formation of macrosteps (deflection image).

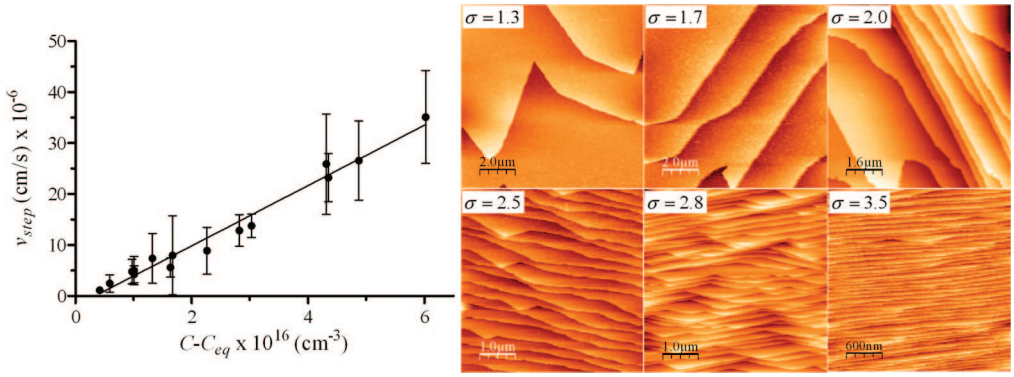

Figure 4. Step growth velocities as measured with AFM. The slope of the linear fit is the step kinetic coefficient $\beta_{step} = 1.2 \times 10^{-3}$ cm/s. AFM images on the right demonstrate the gradual but steady decrease in terrace width as a function of supersaturation.

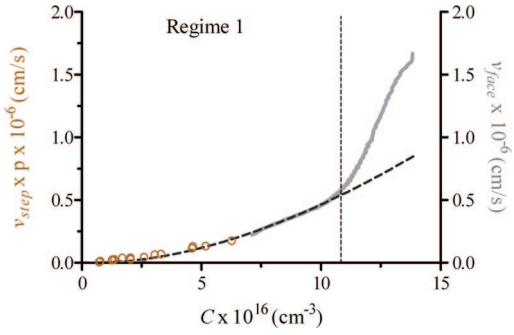

Figure 5. Growth face velocities for the (001) crystal face of glucose isomerase. AFM step velocities were multiplied with the measured crystal slope *p* (open circles), face kinetics obtained using MZI (solid line) and theoretical fit using eq 2 (dashed line).

eventually cease to exist. We found no models in the literature that describe step spacing as a function of supersaturation for the protein crystallization from solution dominated by 2D nucleation. For spiral growth from a vapor phase on F-faces, such a graph is predicted to follow a $\sigma^{1/3}$ dependence.[3] For our data, no power law dependence could be fitted. The empirical curve does however follow a first-order exponential decay for $\sigma < 3$ (Figure 7a).

We can make a rough estimate of the number of macromolecules N^* in the critical nucleus at the transition supersaturation σ_R using the following equation[41]

$$N^* = \frac{\pi\gamma^2}{(k_B T \sigma_R)^2} \tag{3}$$

For $\sigma_R = 5.0 \pm 0.1$ and $\gamma = 1.43 \pm 0.01 \times 10^{-13}$ erg/molecule, we obtain for $N^* \sim 1.5$. This agrees well with the assumption that the kinetic roughening transition is characterized by a critical nucleus with the size of a few molecules or smaller.

Linear Growth Kinetics beyond the Transitioning Supersaturation. Whereas continuous growth is a kinetic phenomenon occurring on the already existing crystal surface, a three-dimensional (3D) analogue of this process exists, that is, spinodal decomposition.[43] It takes place at higher supersaturations, below the metastability/instability boundary. In this regime, the free energy barrier for (3D) nucleation vanishes and infinitesimal density fluctuations can give rise to the appearance

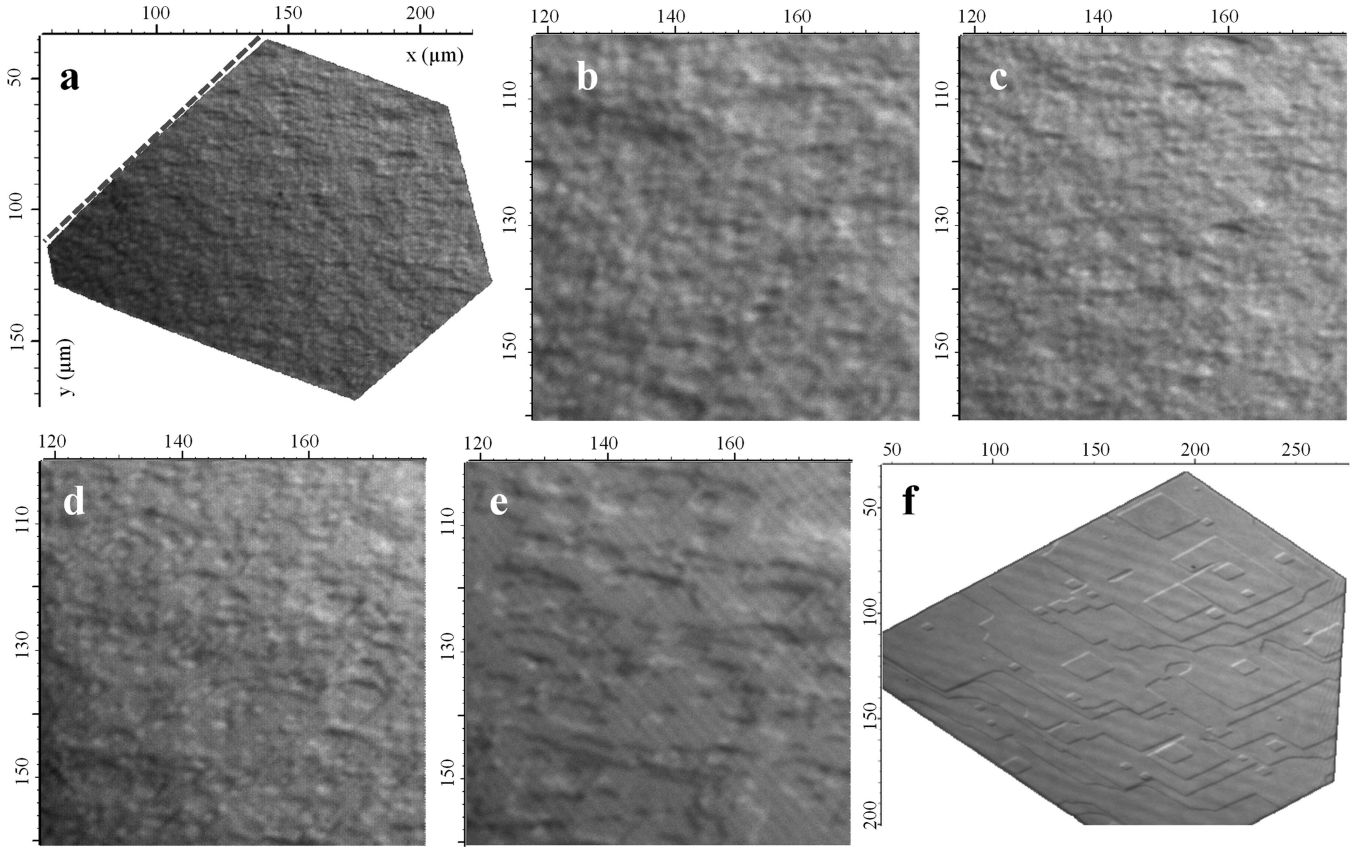

Figure 6. Photomicrographs of a (011) growing glucose isomerase crystal face taken 1.6 h (a), 3.1 h (b), 4.8 h (c), 6.5 h (d), 13.5 h (e) and approximately 24 h (f) after sample preparation. Initial conditions were 30 mg/mL glucose isomerase and 5% PEG 1000. Because of protein bulk depletion the dominating growth mechanism of (011) face switches from kinetic roughening (a) to 2D nucleation (f). Straight dotted line shows crystal face rounding in (a).

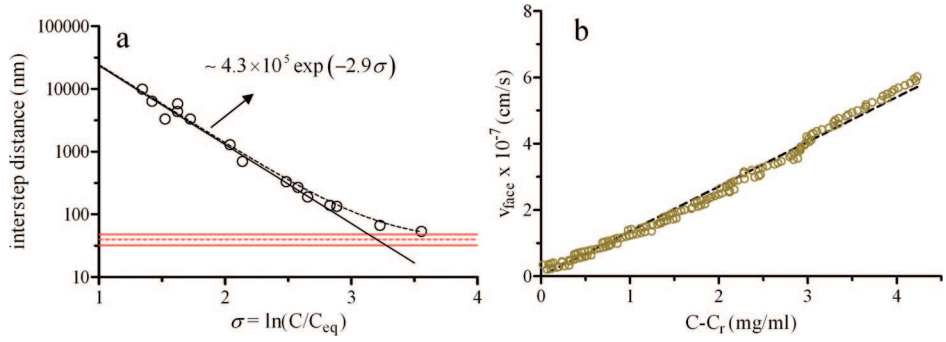

Figure 7. (a) Interstep distance as a function of supersaturation (open circles) and guide for the eyes (dashed line). Best fit was obtained for a first-order exponential decay (goodness of fit $R^2 = 0.9273$, full black line). Red dashed line indicates the static mean excursion of an isolated step, and full red lines show the 95% confidence interval. (b) Face growth velocities as a function of protein concentration above the roughening concentration C_r (open circles), and the dashed line indicates a theoretical fit based on eq 4.

of the new phase.[44,45] Consequently, the generation of the new phase is not delayed, nucleation is instantaneous and the rate of generation is limited by the rate of transport of mass and energy.[46] To rule out the possibility that spinodal decomposition is a possible explanation for the linear kinetics at $\sigma_R > 5.0$, the presence of a solution cloud point for the used conditions was examined. For the temperature range 1−40 °C, no clouding was observed microscopically for the condition: 40 mg/mL glucose isomerase, 100 mM Hepes pH 7.0, 200 mM $MgCl_2$, and 5% PEG1000. Therefore, we conclude that spinodal decomposition does not contribute to the observed linear kinetics at high supersaturations.

As mentioned previously, eq 2 fails to predict the measured face kinetics at high supersaturation levels. We therefore test the hypothesis of kinetic roughening by modeling our results with the expression[30]

$$v_{face}(C,T) = \frac{N_A D_b a^2}{1.6 M_W \varphi^{-1/3}}(C - C_R(T)) \exp(-E_c/k_B T) \quad (4)$$

with a^2 the area of the lattice site, D_b the bulk diffusivity, M_W the molecular weight, φ the macromolecular volume fraction, C and $C_R(T)$ the protein and roughening concentration, respec-

tively, at a given temperature and E_c the energy barrier for the continuous growth process (erg/molecule). As shown in Figure 7b, a clear linear relationship is observed, from which the energy barrier E_c was determined to be $3.74 \pm 0.01 \times 10^{-13}$ erg/molecule (goodness of fit $R^2 = 0.9896$). This linear relationship is a strong indication that kinetic roughening is a likely explanation for the observed face kinetics.

Rounding of Crystal Facets at Supersaturations Larger than σ_R. For the supersaturation range of regime 2, morphological rounding of crystal facets was observed with LCM-DIM (Figure 6a). This rounding of the crystal facets corroborates the hypothesis of kinetic roughening for elevated supersaturation levels.

Conclusion

In this paper we examined two different growth mechanisms for the protein glucose isomerase, that is, 2D nucleation and continuous growth. In general, for the case of 2D nucleation, the size of the critical 2D nucleus is inversely proportional to the temperature and the supersaturation.[47,48] Hence, at a constant temperature T below the roughening temperature T_R, a critical supersaturation σ_R will exist for which the barrier for 2D nucleation essentially vanishes and the size of the critical 2D nucleus is reduced to the order of a growth unit. At such elevated supersaturation levels, individual molecules can become nuclei and lose their surface mobility, and the discrete character of steps is replaced by a more general diffuse roughness of the surface. The kinetics of growth now follow a linear relationship with the supersaturation, and the rate determining step is the delivery of new growth units to the surface, dominated by bulk diffusion. This continuous growth mode is obtained through the kinetic roughening transition. Although the existence of kinetic roughening is well established for small molecules,[23−28] very little data are present in the literature to prove this model's applicability for macromolecular crystal growth.[30,31] Hence we studied the growth mechanism of glucose isomerase at elevated supersaturation levels. Using LCM-DIM the continuous growth mechanism and its transition into 2D nucleation was visualized. The data presented in this paper satisfy all criteria for kinetic roughening. We therefore conclude that glucose isomerase transitions gradually from a 2D nucleation layer generating mechanism to continuous growth around $\sigma_R \simeq 5.0$ at 20 °C. Also, morphological rounding of the crystal facets was observed. From the linear kinetics at $\sigma > \sigma_R$, we estimate the energy barrier for continuous growth to be $3.74 \pm 0.01 \times 10^{-13}$ erg/molecule at 20 °C, which is of the same order as the value obtained for lysozyme ($6.1 \pm 0.4 \times 10^{-13}$ erg/molecule).[30]

Acknowledgment. We thank P. Vekilov for helpful critical discussions. This work was supported by the Flanders Interuniversity Institute for Biotechnology (VIB), the Research Council of the VUB and the Belgian Federal Science Policy Office (DWTC). We thank the European Space Agency for financing in the context of Prodex project AO2004.

References

(1) Hartman, P.; Perdok, W. G. *Acta Crystallogr.* **1955**, *8*, 49–52.
(2) Hartman, P. In *Crystal Growth: An Introduction*; Hartman, P., Eds.; North-Holland: Amsterdam, 1973.
(3) Markov, I. V. In *Crystal Growth for Beginners: Fundamentals of Nucleation, Crystal Growth and Epitaxy*; Markov, I. V., Eds.; World Scientific Publishing: Singapore, 2003.
(4) Malkin, A. J.; Land, T. A.; Kuznetsov, Y. G.; McPherson, A.; DeYoreo, J. J. *Phys. Rev. Lett.* **1995**, *75*, 2778–2781.
(5) Land, T. A.; Malkin, A. J.; Kuznetsov, Y. G.; McPherson, A.; De Yoreo, J. J. *Phys. Rev. Lett.* **1995**, *75*, 2774–2777.
(6) Malkin, A. J.; Kuznetsov, Y. G.; Land, T. A.; De Yoreo, J. J. *Nat. Struct. Biol.* **1995**, *2*, 956–959.
(7) McPherson, A. In *Crystallization of Bilogical Macromolecules*; Bianco, C., Eds.; Cold Spring Harbor Laboratory Press: New York, 1999.
(8) Yau, S. T.; Vekilov, P. G. *Nature* **2000**, *406*, 494–497.
(9) Reviakine, I. *J. Am. Chem. Soc.* **2003**, *125*, 11684–11693.
(10) Burton, W. K.; Cabrera, N.; Frank, F. C *Philos. Trans. R. Soc. Lond.* **1951**, *243*, 299–358.
(11) Jackson, K. A. In *Growth and Perfection of Crystals*; Doremus, R. H., Roberts, B. W., Turnbull, D., Eds.; Chapmann and Hill: London, 1958.
(12) Nielsen, A. E. In *International Series of Monographs on Analytical Chemistry*; Belcher, R., Gordon, L., Eds.; Pergamon: New York, 1964; *Vol. 1*.
(13) Weeks, J. D. In *Ordering in Strongly Fluctuating Condensed Matter Systems*; Riste, T., Eds.; Plenum Press: New York, 1986.
(14) Elwenspoek, M. *J. Phys. A: Math. Gen.* **1987**, *20*, 669–678.
(15) Malkin, A. J.; Chernov, A. A.; Alexeev, I. V. *J. Cryst. Growth* **1989**, *97*, 765–769.
(16) Garcia-Ruiz, J. M. *J. Struct. Biol.* **2003**, *142*, 22–31.
(17) Buckley, H. E. *Crystal Growth*; John Wiley and Sons: New York, 1951.
(18) Hwa, T.; Kardar, M.; Paczuski, M. *Phys. Rev. Lett.* **1990**, *66*, 441–444.
(19) Elbaum, M. *Phys. Rev. Lett.* **1991**, *67*, 2982–2985.
(20) Mutaftschiev, B. In *Handbook of Crystal Growth*; Hurle, D. T. J., Eds.; North-Holland: Amsterdam, 1993; Vol. 1a.
(21) Liu, X.-Y.; van Hoof, P.; Bennema, P. *Phys. Rev. Lett.* **1993**, *71*, 109–112.
(22) Izumi, K. ; Gan Ping; Hashimoto, M.; Toda, A.; Miyaji, H.; Miyamoto, Y.; Nakagawa, Y. In *Advances in the Understanding of Crystal Growth Mechanisms*; Nishinaga, T., Nishioka, K., Harada, J., Sasaki, A., Takei, H., Eds.; North-Holland: Amsterdam, 1997.
(23) Laudise, R. A. *J. Am. Chem. Soc.* **1959**, *81*, 562–566.
(24) Laudise, R. A.; Ballman, A. A. *J. Am. Chem. Soc.* **1958**, *81*, 2655–2657.
(25) Laudise, R. A.; Ballman, A. A. *J. Phys. Chem.* **1960**, *64*, 688–691.
(26) Kolb, E. D.; Laudise, R. A. *J. Am. Ceram. Soc.* **1966**, *49*, 302–305.
(27) Jetten, L. A. M. J.; Human, H. J.; Bennema, P.; van der Eerden, J. P. *J. Cryst. Growth* **1984**, *68*, 503–516.
(28) Liu, X.-Y.; Bennema, P. *J. Cryst. Growth* **1994**, *139*, 179–189.
(29) Durbin, S. D.; Feher, G. *J. Cryst. Growth* **1986**, *76*, 583–592.
(30) Gorti, S.; Forsythe, E. L.; Pusey, M. L. *Cryst. Growth Des.* **2004**, *4*, 691–699.
(31) Gorti, S.; Forsythe, E. L.; Pusey, M. L. *Cryst. Growth Des.* **2005**, *5*, 473–482.
(32) Carrell, H. L.; Glusker, J. P.; Burger, V.; Manfre, F.; Tritsch, D.; Biellmann, J.-F. *Proc. Natl. Acad. Sci. U.S.A.* **1989**, *86*, 4440–4444.
(33) Hariharan, P.; Oreb, B. F.; Eiju, F. *Appl. Opt.* **1987**, *26*, 2504–2505.
(34) Chernov, A. A. In *Modern Crystallography III. Crystal Growth*; Springer-Verlag: Berlin, 1984.
(35) Otalora, F.; Garcia-Ruiz, J. M.; Carotenuto, L.; Castagnolo, D.; Novella, M. L.; Chernov, A. A. *Acta Crystallogr. D* **2002**, *58*, 1681–1689.
(36) Van Driessche, A. E. S.; Sazaki, G.; Otalora, F.; Gonzalez-Rico, F. M.; Dold, P.; Tsukamoto, K.; Nakajima, K. *Cryst. Growth Des.* **2007**, *7*, 1980–1987.
(37) Garcia-Ruiz, J. M.; Novella, M. L.; Moreno, R.; Gavira, J. A. *J. Cryst. Growth* **2001**, *232*, 165–172.
(38) Gavira, J. A.; Garcia-Ruiz, J. M. *Acta Crystallogr. D Biol. Crystallogr.* **2002**, *58*, 1653–1656.
(39) Vekilov, P. G.; Alexander, J. I. D. *Chem. Rev.* **2000**, *100*, 2061–2089.
(40) Malkin, A. J.; Kuznetsov, Y. G.; McPherson, A. *J. Cryst. Growth* **2001**, *232*, 173–183.
(41) Saito, Y. *Statistical Physics of Crystal Growth*; World Scientific: Singapore, 1996; p 9.
(42) Veenendaal, E. v.; van Hoof, P. J; C, M.; van Suchtelen, J.; van Enckevort, W. J. P.; Bennema, P *J. Cryst. Growth* **1999**, *198/199*, 22–26.
(43) Cahn, J. W.; Hilliard, J. E. *J. Chem. Phys.* **1958**, 28.
(44) Shah, M.; Galkin, O.; Vekilov, P. G. *J. Chem. Phys.* **2004**, *121*, 7505–7512.
(45) Filobelo, L. F.; Galkin, O.; Vekilov, P. G. *J. Chem. Phys.* **2005**, *123*, 014904-1−014904-7.
(46) Vekilov, P. G. *Cryst. Growth Des.* **2004**, *4*, 671–685.
(47) Stranski, I. N.; Kaischew, R. I. Z. *Phys. Chem. B* **1934**, *26*, 100–113.
(48) Kaischew, R.; Stranski, I. N. *Z. Phys. Chem. B* **1937**, *34*, 427–432.
CG701220T